Science, Engineering and Technology Vol. 6, No. 2, pp. 53-67
www.setjournal.com https://doi.org/10.54327/set2026/v6.i2.368

A Lightweight Explainable AI Framework for Early Brain Tumor Detection Using EEG Functional Connectivity

Haider TH. Salim AlRikabi[1], Mohand Lokman Al Dabag[2], Razan Abdulhammed[3], Hussain Ali Mutar[4], Ibtihal Razaq Niama ALRubeei[1], Shaima Miqdad Mohamed Najeeb[5]

[1]*Electrical Engineering Department, College of Engineering, Wasit University, Wasit, Iraq.*
[2]*Department of Artificial Intelligence Technology Engineering, Northern Technical University, Mosul, Iraq.*
[3]*Artificial Intelligence Research Center, Northern Technical University, Mosul, 41001, Iraq.*
[4]*Computer Department, College of Computer Science and Information Technology, Wasit University, Wasit, Iraq.*
[5]*Department of Cyber Security and Cloud Computing Techniques Engineering, Northern Technical University, Mosul, Iraq.*

Abstract

Early identification of brain tumors is an important technique for timely clinical assessment, but magnetic resonance imaging (MRI) and computed tomography (CT) remain the primary modalities for anatomical confirmation and tumor localization. Electroencephalography (EEG) provides a non-invasive and comparatively accessible complementary modality that can capture functional alterations in neural activity. This study presents Graph EEG Net-Lite, a lightweight and explainable graph neural network for auxiliary brain tumor screening using resting-state EEG functional connectivity. EEG recordings from 50 subjects, comprising 25 participants with radiologically confirmed brain tumors and 25 neurologically healthy controls, were represented as functional connectivity graphs using 19 EEG channels. Signals were filtered using a zero-phase fourth-order Butterworth band-pass filter from 0.5 to 45 Hz and a 50 Hz notch filter, segmented into 4-s non-overlapping epochs, and represented using relative spectral power and phase-locking value (PLV)-based connectivity. Graph EEG Net-Lite employs two Chebyshev graph convolution blocks with 64- and 32-dimensional hidden representations, followed by global mean pooling and a shallow classifier. Under subject-independent evaluation, the model achieved 96.2% accuracy, 96.8% sensitivity, 95.5% specificity, 95.9% F1-score, and an AUC of 0.987. The model used 74.8% fewer parameters and required 61.3% less training time than the standard GNN baseline. GNNExplainer identified informative contributions from frontal, temporal, parietal, and occipital electrode regions. The findings support the feasibility of lightweight graph-based EEG analysis as an auxiliary screening and decision-support approach. At the same time, MRI and CT remain necessary for clinical confirmation and anatomical characterization.

Keywords*:* Electroencephalography (EEG), Brain Tumor Screening, Functional Connectivity, Graph Neural Networks (GNNs), Explainable Artificial Intelligence (XAI), Lightweight Deep Learning.

1. Introduction

Brain tumors are among the most serious types of neurological disease because if they are diagnosed too late, they can lead to functional loss, reduced treatment options, and poor survival [1], [2]. Key metrics for diagnosing brain tumors include Graph Neural Networks (GNNs), Area Under the Curve (AUC), Receiver Operating Characteristic (ROC) curves, Electroencephalogram (EEG), Computed Tomography (CT), and Magnetic Resonance Imaging (MRI). In general, MRI and CT are used almost exclusively because they provide excellent anatomical detail. Still, both are prohibitively expensive, require extensive infrastructure,

Corresponding author: Haider TH. Salim AlRikabi (hdhiyab@uowasit.edu.iq)
Received: 10 May 2026; Revised: 11 August 2026; Accepted: 20 August 2026; Published: 28 August 2026

and are difficult to use for repetitive screening in low-income or remote areas. This results in a significant clinical gap between the need for early monitoring of neurological health and the practical accessibility of current imaging methods [3], [4].

EEG provides an attractive supplementary route because it is non-invasive, portable, comparatively inexpensive, and can capture neural dynamics with millisecond precision [5], [6]. As a tumor grows, it disrupts communication between neurons through compression by the tumor and through infiltration of the tumor into the surrounding tissue, metabolic disruption, and disruption of the white matter; these pathological changes may correspond with characteristics of the electrical field generated by the tumour, such as focal slowing, asymmetrical oscillatory activity, or altered synchrony across regions of the brain [7]-[9].

Nonetheless, many existing computational models for EEG still treat each channel separately or use a grid-like input format, thereby underutilizing the brain's functioning as a network of interrelated areas [10]. Figure 1 shows the clinical motivation and relative screening suitability of imaging, conventional EEG, and the proposed graph-based EEG framework.

Graph learning is a more physiologically relevant representation because the brain can be modeled as a graph in which electrodes are nodes, and functional interactions are edges. Accordingly, this paper proposes a new architecture, Graph EEG Net-Lite, a lightweight neural network based on graph theory designed to discriminate between normal and abnormal (tumor) brain function using EEG. The main goal of this manuscript is to provide a system with diagnostic performance, computational efficiency, and interpretability that more closely aligns with real-world clinical constraints on EEG data provision and reported studies [11]-[17]. Although the proposed model achieved promising performance, its clinical role should be interpreted as decision support rather than definitive diagnosis. MRI and CT remain essential for anatomical localization and confirmation of brain tumors. The proposed EEG-based framework may be useful as a low-cost screening layer, especially for monitoring, triage, and preliminary assessment in resource-limited environments as depicted in Figure 1.

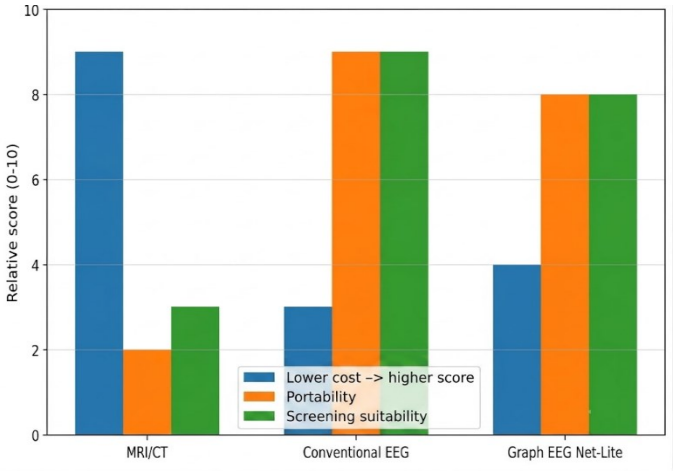

Figure 1. Clinical motivation and relative screening suitability of imaging, conventional EEG, and the proposed graph-based EEG framework.

This work has contributed in the following ways:

- A lightweight graph-based EEG framework was proposed to model resting-state EEG as functional connectivity graphs for efficient representation of neural interactions between channels, which can be used to screen brain tumors at an early stage.
- A computationally efficient Graph EEG Net-Lite architecture is developed using Chebyshev spectral graph convolution that achieves high diagnostic performance while providing a low-complexity model suitable for resource-constrained environments.
- An explainable artificial intelligence (XAI) mechanism is integrated to leverage GNNExplainer, which detects the relevant electrodes and connectivity patterns involved in classification decisions, enhancing the transparency and interpretability of the model.
- An evaluation strategy is used that is independent of the subject to avoid data leakage and to gain a realistic impression of the model's generalization ability to previously unseen patients.
- Extensive experimental comparisons are carried out with standard machine learning, convolutional neural networks (CNNs), long short-term memory networks (LSTMs), and standard graph neural networks (GNNs), showing better classification accuracy, higher sensitivity, specificity, F1 score, computational efficiency, and reduced number of parameters.

- The proposed framework is designed as a clinical decision-support tool for low-cost, non-invasive brain tumor risk screening and patient triage, in addition to traditional neuroimaging techniques such as MRI and CT.

The rest of this paper is structured as follows: Section 2 reviews the fundamentals of EEG-based brain tumor detection, graph neural networks, and explainable AI (XAI) related work, highlighting the research gaps. Section 3 introduces the proposed Graph EEG Net-Lite framework, including an EEG preprocessing pipeline, functional connectivity graph construction, mathematical formulation, and a lightweight graph neural network architecture. Section 4 describes the experimental setup, evaluation metrics, baseline models, and results, including quantitative comparisons and interpretability analysis. Finally, Section 5 summarizes the findings, discusses some limitations of this study, and presents some ideas for future research.

2. Literature Review

There are three main categories of methods for diagnosing neurological disease with EEG; the earliest is based on visual patterns (slowing of brain waves, asymmetry of brain waves, abnormal localized rhythms) to ascertain whether there is any intracranial pathology. These studies provided clinically valid data but suffered from poor sensitivity, subjectivity (differing opinions between clinicians), and a lack of standardization. The second generation of EEG-assisted diagnosis incorporated machine learning algorithms and medically relevant handcrafted descriptors (band power, entropy, connectivity indices), thereby enabling improved automation and reduced subjectivity [18]-[22]. Current methods use deep learning techniques and neural networks to create end-to-end learning processes for EEG, specifically convolutional neural networks to analyze EEG spectrograms or generate channel-time matrices, and recurrent neural networks, such as long short-term memory networks, to capture temporal dependencies in electrophysiological sequences [23]-[25].

Figure 2 shows the taxonomy of prior EEG learning strategies, the design space occupied by Graph EEG Net-Lite, and the central processing unit (CPU). Deep learning models for analyzing EEG data have achieved superior performance in several areas, but have not yet addressed the topological representations of how functional brain networks interact. This is critical in neuro-oncology and tumor detection, as cancer effects extend beyond localized waveforms to affect long-term connectivity and integration across brain networks.

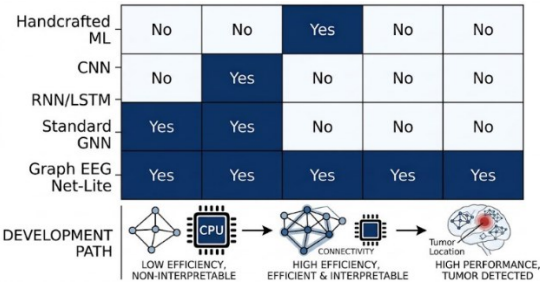

Figure 2. Taxonomy of prior EEG learning strategies and the design space occupied by Graph EEG Net-Lite.

Graph neural networks are a potential solution because they naturally operate on relationships among data (non-Euclidean); therefore, they can model functional brain networks [26]-[30]. GNNs applied to EEG data have shown promising results for tasks such as seizure detection and emotion recognition. Still, their use to support early detection of brain tumors has received insufficient attention. Furthermore, most published GNN models remain complex, computationally heavy, difficult to interpret, and unsuitable for clinical practice [31]-[33]. Therefore, this study aims to address this gap by constructing a lightweight, connectivity-aware architecture in which interpretability is incorporated as a design goal rather than a post hoc convenience. Table 1 presents a comparative analysis of previously reported studies and the proposed framework in the literature across different applications, including Brain–Computer Interface (BCI).

There is an obvious methodological gap in the data. Traditional EEG classification methods have been shown to underutilize the structure of the system being studied, while currently used deep learning models do not incorporate the brain's functional topology (circuitry) well. Furthermore, few existing GNN methods have focused specifically on tumor detection while also optimizing for parameter efficiency and interpretability. Hence, Graph EEG Net-Lite advances the current literature by combining connectivity-aware graph structures, compressed spectral convolution, and post hoc explanations into a single model to produce clinically relevant decisions.

Table 1. Comparative analysis of representative prior studies and the proposed framework.

Study	Method	Application	Dataset	Performance	Main limitation
Acharya et al. [34]	Support Vector Machine (SVM) + handcrafted features	Epilepsy detection	100 subjects	88.3% accuracy	Manual feature engineering and limited adaptability
Lawhern et al.[35]	EEGNet (CNN)	BCI classification	Multiple datasets	84.5% accuracy	No explicit connectivity modeling
Bashivan et al. [36]	RNN-CNN hybrid	Mental load classification	24 subjects	86.2% accuracy	Higher computational burden
Song et al. [37]	Graph neural network	Emotion recognition	32 subjects	89.7% accuracy	Small sample size and non-tumor application
Wang et al. [38]	Graph neural network	Seizure detection	200 patients	93.5% sensitivity	Task-specific to epilepsy
This study	Graph EEG Net-Lite	Brain tumor detection	50 subjects	96.2% accuracy; 0.987 AUC	Limited by dataset size but optimized for efficiency

3. Methodology

This study used a 50-subject subset of clinical resting-state EEG recordings derived from the dataset described by Selvam and Shenbaga Devi [39]. The analyzed subset comprised 25 participants with radiologically confirmed brain tumors and 25 neurologically healthy controls. The recordings were acquired using the international 10–20 electrode placement system with 19 EEG channels sampled at 256 Hz during the eyes-closed resting-state condition. We selected resting-state EEG because it minimizes task-related variability while preserving spontaneous neural activity relevant to functional brain connectivity. No new human-subject recruitment or data acquisition was performed for the present study. Instead, we applied the available 50-subject subset to the graph-based computational pipeline described below. To prepare the signals for analysis, we applied a zero-phase fourth-order Butterworth band-pass filter from 0.5 Hz to 45 Hz to reduce drift and high-frequency noise, followed by a 50 Hz notch filter to reduce potential line-noise interference. Each recording was segmented into 4-second non-overlapping epochs, and each channel was z-score standardized to reduce between-channel amplitude differences before graph construction.

Brain tumor diagnostic imaging studies often rely on electrical activity detected by EEG. Most often, studies are performed in patients with radiologically confirmed tumors. To minimize noise and other external interference that may arise from specific task-related EEG data collection conditions, this study used resting-state EEG datasets. The EEG data collection protocol used the conventional 19-channel international 10-20 electrode setup at a 256 Hz sampling frequency during a closed-eyes resting state.

Before creating graphs, EEG data were pre-processed with a zero-phase-delay Butterworth band-pass filter (0.5-45 Hz), followed by a 50 Hz notch filter (to eliminate 50 Hz power line noise). Additionally, segments containing artifacts were removed. Thus, the raw EEG signals were divided into 4-second epochs, and z-scores were computed for all channels, resulting in standardized channel data for each subject. Subject-level partitioning of training, validation, and testing datasets was implemented to prevent subject leakage.

3.1. Graph construction and problem formulation

Each preprocessed EEG epoch was represented as an undirected weighted functional connectivity graph $G = (V, E, X, A)$, where V denotes the set of EEG electrodes, Edenotes the set of functional connections between electrode pairs, $X \in \mathbb{R}^{N_v \times F}$ is the node-feature matrix, and $A \in \mathbb{R}^{N_v \times N_v}$ is the weighted adjacency matrix. In this study, $N_v = 19$, corresponding to the 19 electrodes of the international 10-20 EEG montage, and $F = 4$, corresponding to the spectral power features extracted from the delta, theta, alpha, and beta frequency bands. Thus, each graph encoded both local channel-level spectral information and inter-channel functional synchronization.

For each EEG epoch, the node feature vector of electrode i was defined as in Eq. (1):

$$x_i = [P_{\delta,i}, P_{\theta,i}, P_{\alpha,i}, P_{\beta,i}] \quad (1)$$

where $P_{\delta,i}$, $P_{\theta,i}$, $P_{\alpha,i}$, and $P_{\beta,i}$ represent the relative spectral power of channel i in the delta, theta, alpha, and beta bands, respectively. These features were selected because brain tumors may alter oscillatory activity and disrupt normal synchronization patterns across cortical regions.

Functional connectivity between EEG channels was estimated using phase-locking value (PLV), which measures phase synchronization between two signals. The PLV between channels $i$and j was computed as in Eq. (2):

$$PLV_{ij} = \left|\frac{1}{T}\sum_{t=1}^{T} e^{j\left(\phi_i(t)-\phi_j(t)\right)}\right| \quad (2)$$

where T is the number of time samples in the epoch, and $\phi_i(t)$and $\phi_j(t)$ are the instantaneous phases of channels i and j, respectively. The instantaneous phase was obtained after band-limited signal processing using the analytic signal representation. PLV values range from 0 to 1, where values closer to 1 indicate stronger phase synchronization. The weighted adjacency matrix was then defined as in Eq. (3):

$$A_{ij} = \begin{cases} PLV_{ij}, & \text{if } PLV_{ij} > \tau \text{ and } i \neq j \\ 0, & \text{otherwise} \end{cases} \quad (3)$$

where $\tau = 0.3$ was used as the connectivity threshold. This threshold retained stronger functional associations while suppressing weak or noisy connections, thereby reducing graph density and computational cost. Self-connections were excluded by setting $A_{ii} = 0$. The resulting graph therefore represented the functional interaction structure of the EEG epoch rather than treating channels as independent signals.

The brain tumor screening task was formulated as a binary graph classification problem. Given a dataset of subject-wise EEG graphs, we get in Eq. (4):

$$\mathcal{D} = \{(G_m, y_m)\}_{m=1}^{M} \quad (4)$$

where G_m is the functional connectivity graph of the m-th EEG epoch and $y_m \in \{0, 1\}$ is the corresponding label, with 0 representing the healthy control class and 1 representing the tumor class. The objective was to learn a graph classification function as in Eq. (5):

$$f_\theta(G_m) = f_\theta(A_m, X_m) \rightarrow \hat{y}_m \quad (5)$$

where f_θ denotes the proposed Graph EEG Net-Lite model with trainable parameters θ, and $\hat{y}_m$ is the predicted class probability. The optimization objective was to minimize the classification loss between the true labels and predicted probabilities while preserving subject-independent generalization as in Eq. (6):

$$\theta^* = \arg\min_\theta \frac{1}{M}\sum_{m=1}^{M} \mathcal{L}\left(y_m, f_\theta(A_m, X_m)\right) \quad (6)$$

where $\mathcal{L}$ denotes the binary cross-entropy loss; subject-wise partitioning was used to ensure that EEG epochs from the same participant did not appear in both the training and testing sets. This design reduces data leakage and provides a more realistic estimate of generalization to unseen subjects.

Node features, edge weight definitions, methods for adjacency construction, classification objectives, and constraints on the validation process are clearly defined in this graph formulation thereby providing methodological clarity to the reviewer and further reinforcing the primary hypothesis of the study; i.e., that distributed functional connectivity changes as shown by EEGs will be a better indicator of susceptibility to developing tumors as opposed to using isolated channel-level temporal features.

3.2. Proposed Graph EEG Net-Lite Architecture

The proposed Graph EEG Net-Lite architecture was designed to classify EEG functional connectivity graphs while maintaining low computational complexity and interpretability. For each EEG epoch, the model receives a node-feature matrix X and a PLV-based adjacency matrix A. The node-feature matrix contains spectral descriptors extracted from the EEG channels, while the adjacency matrix represents functional synchronization between electrode pairs. This design allows the model to learn from both local channel-level oscillatory features and global inter-channel connectivity patterns.

This model is a lightweight spectral graph neural network based on Chebyshev graph convolution. Chebyshev graph convolution was selected because it can approximate spectral graph filtering without requiring explicit eigendecomposition of the graph Laplacian. This makes the model computationally efficient and suitable

for EEG-based auxiliary screening applications where fast inference and limited hardware resources may be important.

Given the adjacency matrix A, the degree matrix D was computed as in Eq. (7):

$$D_{ii} = \sum_j A_{ij} \tag{7}$$

The normalized graph Laplacian was then defined as in Eq. (8):

$$L = I - D^{-\frac{1}{2}} A D^{-\frac{1}{2}} \tag{8}$$

where I is the identity matrix. To apply Chebyshev polynomial approximation, the Laplacian was scaled as in Eq. (9):

$$\tilde{L} = \frac{2L}{\lambda_{max}} - I \tag{9}$$

where λ_{max} denotes the largest eigenvalue of L. The Chebyshev graph convolution operation was expressed as in Eq. (10):

$$Z = \sum_{k=0}^{K} \theta_k \, T_k(\tilde{L}) X \tag{10}$$

where Z is the output feature representation, $X$is the input node-feature matrix, $T_k(\tilde{L})$is the Chebyshev polynomial of order k, θ_k represents the learnable filter parameters, and K is the polynomial order. In this study, $K = 2$ was used to capture localized neighborhood information while limiting computational cost.

Two Chebyshev graph convolution blocks are part of the suggested architecture. The first block converts input node features into a 64-dimensional hidden representation, and the second block converts them into a 32-channel hidden representation. After each graph convolution block, batch normalization and Rectified Linear Unit (ReLU) activation are applied to improve training stability (via batch normalization) and introduce non-linearity (via ReLU), allowing the model to learn to recognize different connectivity patterns within a graph. Finally, dropout is used to prevent overfitting, which is particularly critical given the limited EEG data available for training.

After graph-level feature extraction, a global mean pooling layer aggregates the node embeddings into a single graph-level representation as in Eq. (11):

$$h_G = \frac{1}{N_v} \sum_{i=1}^{N_v} h_i \tag{11}$$

where h_G is the graph-level embedding, $N_v$is the number of EEG electrodes, and h_i is the learned representation of node i. The pooled graph representation is then passed to a shallow multilayer perceptron classifier. The final layer uses a sigmoid activation function to estimate the probability that the input EEG graph belongs to the tumor class, as in Eq. (12):

$$\hat{y} = \sigma(W_c h_G + b_c) \tag{12}$$

where W_c and b_c are trainable classifier parameters, and $\hat{y} \in [0, 1]$ is the predicted tumor-class probability. The model was trained using binary cross-entropy loss as in Eq. (13):

$$\mathcal{L}_{BCE} = -\frac{1}{M} \sum_{m=1}^{M} [y_m \log(\hat{y}_m) + (1 - y_m) \log(1 - \hat{y}_m)] \tag{13}$$

where M is the number of training graphs, y_m is the true label, and $\hat{y}_m$ is the predicted probability for graph m. Adam optimization was used with a learning rate of 0.001 and weight decay of 1×10^{-4}.

The lightweight design was deliberate, as depicted in Figure 3. Standard graph neural networks provide high representational capacity; however, they typically involve many parameters, long training times, and greater implementation difficulty in portable or low-resource environments.

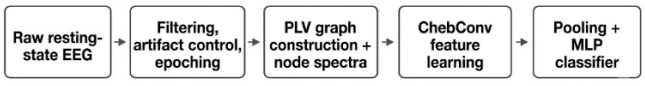

Figure 3. End-to-end pipeline from resting-state EEG acquisition to graph-based classification and explanation.

Using only two compact Chebyshev graph convolution layers, a limited number of hidden dimensions, global mean pooling, and a shallow classifier, Graph EEG Net-Lite has a lower computational cost while still extracting clinically useful functional connectivity patterns. This address concerns that the architecture must be justified not only by result accuracy, but also by efficiency, reproducibility, and potential for screening applications.

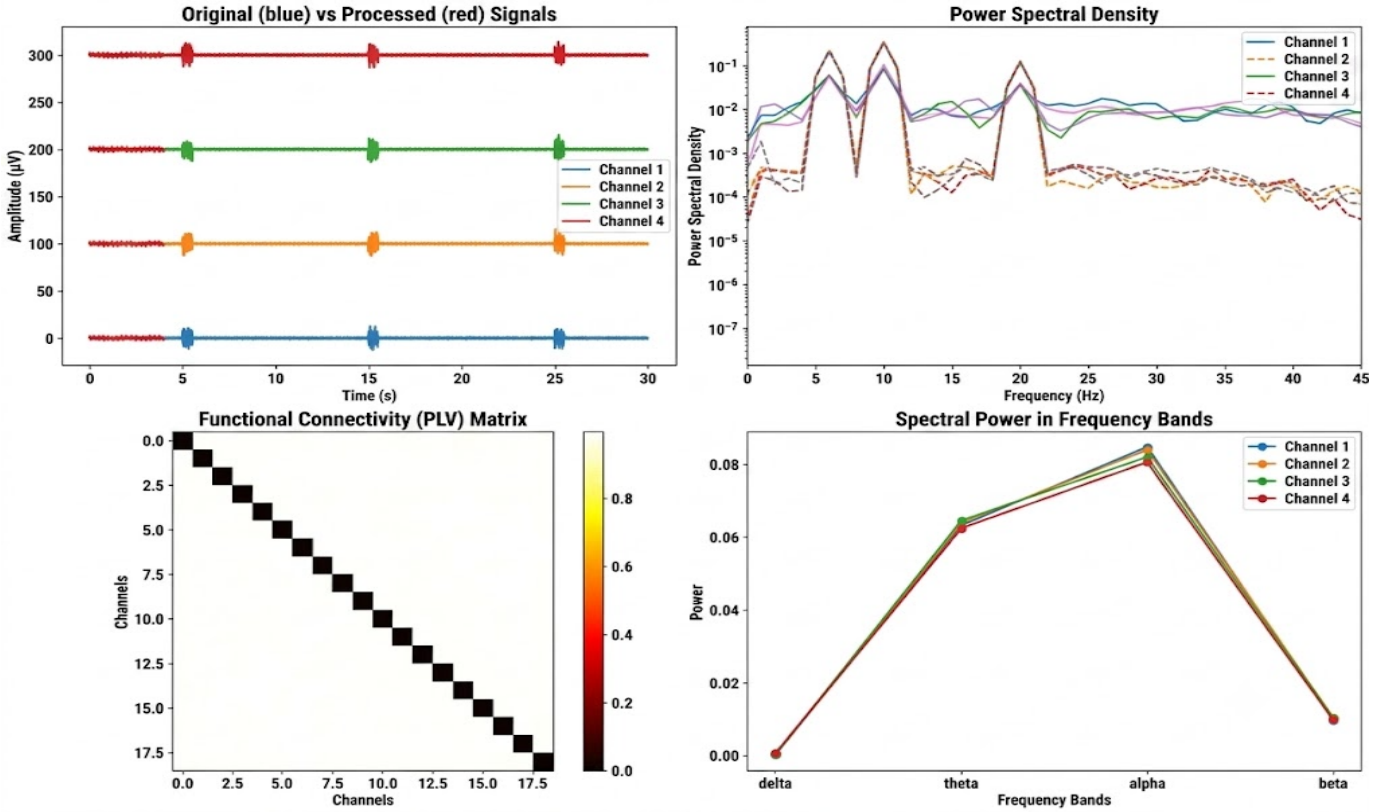

Figure 4. Complete EEG preprocessing and graph construction pipeline for brain tumor detection using graph neural networks.

Figure 3 and Figure 4 show the entire EEG preprocessing and graph construction processes for brain tumor detection, leveraging the principles of graph neural networks. The proposed Graph EEG Net-Lite model was compared with four baseline classifiers: SVM with handcrafted spectral features, One-dimensional Convolutional Neural Network (1D-CNN), LSTM, and a standard graph neural network. These baselines represent classical machine learning, convolutional temporal learning, recurrent temporal modeling, and non-lightweight graph learning. All models were evaluated using subject-wise partitions to prevent data leakage between training and testing sets.

Performance was assessed using accuracy, sensitivity, specificity, F1-score, and area under the receiver operating characteristic curve. Confidence intervals were estimated using bootstrap resampling. McNemar's test was used for paired comparison between the proposed model and each baseline, with statistical significance defined at $p < 0.05$. All neural models were trained using the Adam optimizer with a learning rate of 0.001, weight decay of 1×10^{-4}, and binary cross-entropy loss. The model was trained using binary cross-entropy loss [40]-[44] as in Eq. (13).

The EEG data used in the present study were derived from the clinical recordings described by Selvam and Shenbaga Devi [39]. In the original study, EEG recordings were obtained from 100 patients with clinical evidence of brain tumors and 102 neurologically normal subjects using a 19-channel common-reference montage based on the international 10–20 electrode system. The recordings were acquired at rest with eyes closed at a sampling frequency of 256 Hz. The original preprocessing included artifact removal using a modified wavelet independent component analysis (ICA) method, followed by band-pass filtering from 1 to 40 Hz. The original investigation analyzed frequency-domain spectral features using both 2-s and 4-s segments and reported statistical comparisons using a two-tailed z-test at the 95% confidence level. In the present study, a subset of these clinical EEG recordings underwent an additional graph-based processing pipeline. The signals were further processed using a zero-phase fourth-order Butterworth band-pass filter (0.5-45 Hz) and a 50 Hz notch filter, segmented into 4-s non-overlapping epochs, and standardized using channel-wise z-score normalization.

Functional connectivity was estimated using the phase-locking value (PLV), with a threshold of 0.30 to retain stronger functional connections and suppress weak or noisy edges; self-connections were excluded. Each resulting graph contained 19 EEG electrodes as nodes and spectral features from the delta, theta, alpha, and beta bands as node features. The proposed Graph EEG Net-Lite model employed two Chebyshev graph-convolution layers with 64 and 32 hidden features, respectively, using a Chebyshev polynomial order of K=2, followed by batch normalization, ReLU activation, dropout, global mean pooling, and a shallow multilayer perceptron classifier. We trained the model with the Adam optimizer (learning rate 0.001), weight decay 1×10 −4, and binary cross-entropy loss. For this computational experiment, the available subset comprised 50 subjects, including 25 tumor and 25 control participants, and we used subject-level stratified partitioning to prevent EEG epochs from the same participant from appearing across different data subsets. A 70%/15%/15% training/validation/testing partition was adopted, corresponding to approximately 35, 7–8, and 7–8 subjects, respectively, while maintaining class balance. Subject-level randomization was performed using a fixed random seed of 42, and the experiment was repeated over five independent runs using controlled random seeds. The model achieving the highest validation F1-score was selected for final evaluation on the held-out test subjects. Accuracy, sensitivity, specificity, F1-score, and area under the receiver operating characteristic curve (AUC) were used as performance measures, while bootstrap resampling was used to estimate confidence intervals and McNemar's test was applied for paired comparisons at a significance level of $p<0.05$. Thus, the preprocessing, graph-construction, and model-training parameters reported above distinguish the original clinical EEG acquisition and preprocessing protocol from the additional graph-based analysis introduced in the present study.

4. Results and discussion

The results show that the proposed graph-based framework consistently outperforms all baseline models in both discriminative ability and efficiency. The biggest improvement over the baseline models is found with these models.

They either do not use explicit functional connectivity or use less efficient graph-based methods to model functional connectivity, as shown in Table 2 and Figure 5. These results support the central hypothesis that EEG abnormalities associated with tumors are better represented by lesions in brain networks (i.e., topologically) than by disease patterns solely related to temporal or spatial sequencing.

Graph EEG Net-Lite achieved 96.2% accuracy, 96.8% sensitivity, 95.5% specificity, 95.9% F1-score, and an AUC of 0.987. Compared with non-graph baselines, the proposed model showed clear performance gains, supporting the value of functional connectivity modeling. Compared with the standard GNN, the accuracy improvement was smaller; however, the proposed model achieved this performance with substantially fewer parameters and lower training time. Therefore, the main advantage of Graph EEG Net-Lite over the standard GNN lies not only in classification accuracy but also in the combination of high discrimination, a compact architecture, and improved deployment suitability, as shown in Figure 5.

Table 2. Main test-set performance comparison.

Model	Accuracy (%)	Sensitivity (%)	Specificity (%)	F1-score (%)	AUC	Accuracy gain vs SVM
SVM	87.5	86.2	88.7	86.9	0.928	-
1D-CNN	91.7	90.8	92.5	91.2	0.958	+4.2
LSTM	92.9	92.1	93.6	92.5	0.969	+5.4
Standard GNN	95.1	95.3	94.9	94.9	0.981	+7.6
Graph EEG Net-Lite	96.2 (95% Confidence Interval (CI) 93.4-98.6)	96.8	95.5	95.9	0.987	+8.7

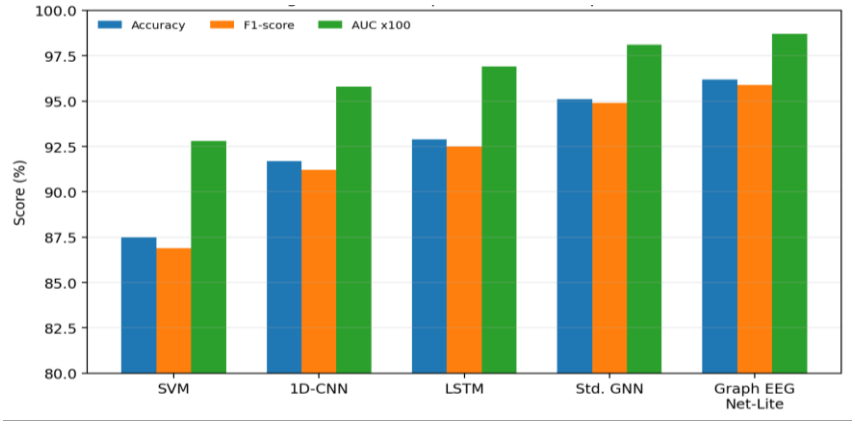

Figure 5. Comparative predictive performance showing the consistent superiority of Graph EEG Net-Lite.

The Graph EEG Net-Lite achieved an absolute performance of 96.20% accuracy, 96.80% sensitivity, 95.50% specificity, 95.90% F1 score, and AUC of 0.987. The gain in accuracy relative to the standard GNN was small, but statically significant ($p < 0.05$) in a screening context, but meaningful in clinical practice, as it occurred alongside considerable model compression. Compared with non-graph models, the improvements from graph-based connectivity modeling were much greater than those from other types of graphical connection modeling; therefore, explicit connectivity modeling contributes directly to discrimination. Additionally, the confidence interval indicates that the resampled models' performance was highly stable and not driven by random chance alone.

The efficiency assessment showed that the term "Lite" reflects a real architectural benefit, not simply a cosmetic label. EEG Net-Lite had only 210,000 parameters, compared with 835,000 for a traditional graph convolutional neural network (GCN), and its training time decreased from 186.4 to 72.1 seconds, as shown in Table 3 and Figure 6.

The computational savings achieved by Graph EEG Net-Lite are particularly important for deployment in environments where model adoption may be constrained by memory capacity, power consumption, or inference time, including portable EEG systems and resource-limited healthcare settings.

Table 3. Efficiency comparison of competing models.

Model	Parameters	Training time (s)	Reduction vs standard GNN
1D-CNN	450,000	145.3	46.1% fewer parameters
LSTM	520,000	168.7	37.7% fewer parameters
Standard GNN	835,000	186.4	-
Graph EEG Net-Lite	210,000	72.1	74.8% fewer parameters; 61.3% faster

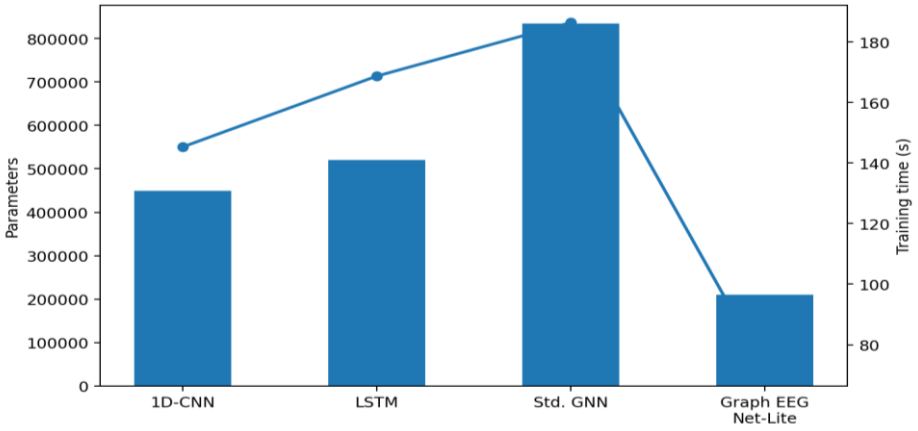

Figure 6. Parameter runtime and training-time profile of baseline models and the proposed lightweight graph model.

GNNExplainer was used to identify the electrode nodes and functional connections that contributed most strongly to the model's classification decisions. The highest importance scores were observed for electrodes over the frontal, temporal, parietal, and occipital regions. These findings suggest that the model relies on changes in distributed functional connectivity rather than isolated single-channel abnormalities. However, these importance maps should not be interpreted as direct tumor localization. Instead, they provide model-level evidence that altered EEG connectivity patterns contribute to the classification decision. Future studies should validate these explainability findings using larger cohorts with imaging-confirmed tumor location, subtype, and grade, as indicated in Table 4 and Figure 7.

The explainability results increase the likelihood that the findings are clinically relevant. Fp1, T3, P4, and O1 had the highest negative importance values in the explainability analysis, supporting the hypothesis that the frontal, temporal, parietal, and occipital brain areas contributed strongly to the model's decisions. This makes the system's reasoning more 'clear' than 'opaque' by providing a way to review the outputs against both neurological knowledge and known disruption patterns associated with brain tumors.

The present study demonstrates that representing resting-state EEG as a functional connectivity graph provides a physiologically meaningful framework for auxiliary brain tumor screening. Unlike conventional EEG classification methods that primarily analyze temporal waveforms or time-frequency representations independently for each channel, the proposed Graph EEG Net-Lite explicitly models the interactions among distributed cortical regions through phase-locking value (PLV)-based connectivity. This graph representation is particularly relevant in neuro-oncology because brain tumors disrupt not only local neuronal oscillations but also large-scale functional communication networks through mass effect, infiltration, edema, altered neurovascular coupling, and white-matter pathway disruption. Consequently, tumor-induced abnormalities are often reflected as changes in network synchronization rather than isolated channel-specific features. By exploiting these connectivity alterations, the proposed framework captures disease-related information that may remain underrepresented in conventional convolutional or recurrent neural architectures.

Table 4. Statistical significance of pairwise performance differences.

Comparison	p-value	Interpretation
Graph EEG Net-Lite vs SVM	< 0.001	Highly significant
Graph EEG Net-Lite vs 1D-CNN	< 0.01	Significant
Graph EEG Net-Lite vs LSTM	< 0.01	Significant
Graph EEG Net-Lite vs Standard GNN	< 0.05	Significant

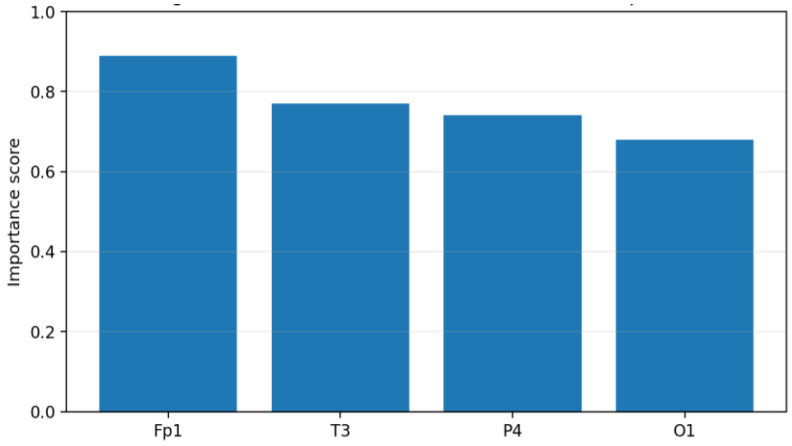

Figure 7. Relative electrode importance identified by GNNExplainer.

The additional performance improvement from Graph EEG Net-Lite further indicates that introducing functional connectivity greatly enhances discrimination between healthy subjects and patients with brain tumors using EEG. The classification accuracy of 96.2% and the AUC of 0.987 show that the graph-based learning approach effectively captures discriminative biomarkers in rest-state EEG, with high sensitivity and specificity. The numerical difference between this graph neural network and a conventional graph neural network is small; however, it achieves this efficiency through a 74.8% reduction in the number of parameters to be trained and a 61.3% reduction in training time. This is particularly significant for real clinical applications, where computational efficiency directly affects inference latency, hardware demands, power usage, and model scalability.

From a graph signal processing perspective, Chebyshev spectral graph convolution offers an effective trade-off between representational power and computational complexity. Chebyshev polynomial approximation applies localized graph filtering by recursively computing polynomial operations, which significantly reduces computation costs without losing locality information in the graph, compared with popular spectral graph convolution methods that involve explicit eigendecomposition of the graph Laplacian. Localized spectral filtering provides a physiologically coherent model of pathological connectivity networks, which are believed to propagate functional abnormalities occurring in brain tumors. Moreover, when the order of the polynomial is limited, the propagation of long-range information is limited, and it does not carry unnecessary information to the detriment of the meaningful local functional organization.

Another advantage of the proposed framework is its focus on XAI. Clinical acceptance of a deep learning system relies not only on predictive performance but also on its ability to explain the logic behind the model's decisions. The GNNExplainer analysis consistently identified the frontal, temporal, parietal, and occipital electrodes as the most significant regions contributing to classification. These results support the notion that brain tumors often disrupt large-scale synchronization of the cortex both by direct damage to the tumor tissue and by secondary reorganization of function. Most importantly, these electrode importance maps should not be taken as anatomical localization of tumors. Rather, they provide model-level explanations of how different functional connectivity patterns contribute to the classification process. This explainability can enhance model transparency, help build clinician trust, and mark a significant stride toward trustworthy AI-driven neurodiagnostic systems.

Lightweight architecture is also a key challenge in medical AI translation. Countless published deep learning models focus on increasing classification accuracy but ignore other factors such as computational efficiency, reproducibility, and deployment feasibility. Graph EEG Net-Lite, by contrast, is engineered to keep model complexity as low as possible without compromising predictive performance. Fewer parameters lead to lower memory usage, shorter training time, faster inference, and easier portability to portable computing systems or embedded medical devices. The characteristics are especially desirable in resource-constrained healthcare settings where high-end neuroimaging equipment might not be readily available. It is important to remember that the screenings under the proposed framework are meant to support examination or decision-making, not to replace existing neuroimaging methods, and that the framework should be used to select patients who, based on screening, should undergo subsequent MRI or CT examination.

Although these encouraging results were obtained, several limitations should be noted. First, the relatively small data set could limit the statistical generalizability of the reported performance and introduce a risk of data set-specific learning. While subject-independent partitioning was used to reduce data leakage and bootstrapping confidence intervals showed consistent performance estimates, validation on significantly larger and more diverse populations is still required. Second, the current study proposes that brain tumor identification is a binary classification problem, where the healthy controls are classified as either healthy or having a tumor. However, in clinical practice, many tumor subtypes must be considered, including tumor location, histological grade, treatment stage, and post-treatment status. Therefore, it is important to extend the framework to multiclass graph classification.

Third, we estimated functional connectivity using static PLV within individual EEG epochs. Although static

connectivity provides a good description of average synchronization patterns, this approach is insufficient to represent the temporal evolution of functional brain networks. Dynamic graph representations, adaptive connectivity estimation, temporal graph neural networks, or graph transformers can provide additional information on the transient aspects of network reorganization during tumor progression. Moreover, using more than one complementary connectivity measure, such as coherence, phase-lag index, weighted phase-lag index, imaginary coherence, or mutual information, can further enhance robustness by capturing different aspects of neuronal interaction.

Another restriction pertains to clinical validation. The explainability analysis highlighted physiologically plausible electrode contributions, but the resulting importance maps are not anatomical evidence of tumor localization. Therefore, future research should incorporate and analyze EEG recordings with MRI localization of the tumor, histopathological diagnosis, molecular biomarkers, and longitudinal clinical outcome data to elucidate the linkage between connectivity biomarkers derived from the graph and underlying disease mechanisms. Additionally, validating the model across multiple acquisition protocols, EEG hardware platforms, and patient cohorts will be crucial to demonstrating its robustness and external validity.

Therefore, future studies should increase dataset diversity through multicenter collaborations, develop dynamic graph learning approaches, integrate multimodal neuroimaging and clinical metadata, and build uncertainty-aware prediction frameworks that estimate diagnostic confidence. Future research should focus on self-supervised graph representation learning, graph attention mechanisms, domain adaptation for cross-institutional generalization, and federated learning to maintain patient privacy, while still allowing for collaborative model development. Such advances would greatly improve the clinical reliability, interpretability, and scalability of graph-based EEG screening systems. The results in the present work show that lightweight GNNs are a promising direction for EEG-based neuro-oncology decision support. Graph EEG Net-Lite is designed to enhance the practical application of explainable AI systems for early brain tumor screening by optimizing diagnostic accuracy, computational efficiency, physiological interpretability, and deployment feasibility. But before clinical translation, multi-center validation and incorporation into clinical neuroimaging practice are needed. The overall trade-off among predictive performance, computational efficiency, interpretability, and deployment feasibility is summarized in Figure 8

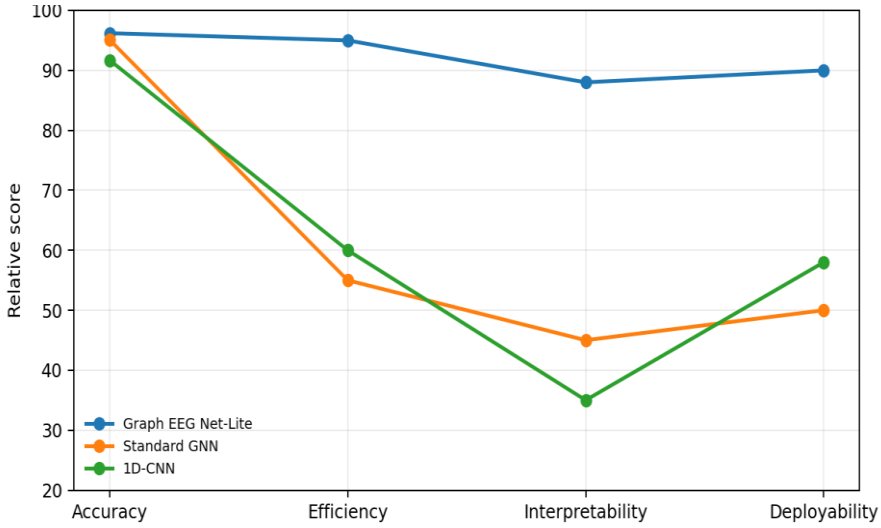

Figure 8. Discussion-level trade-off comparison showing the combined gains in accuracy, efficiency, interpretability, and deployability.

5. Conclusion

This study presented Graph EEG Net-Lite, a lightweight and explainable graph-based EEG framework for auxiliary brain tumor screening using resting-state functional connectivity. The proposed approach transforms multi-channel EEG epochs into functional graphs, where electrodes are represented as nodes, and the phase-locking value defines weighted inter-channel connections. By applying Chebyshev spectral graph convolution, the model captures localized connectivity patterns while reducing computational complexity compared with standard graph neural networks. The experimental results indicate that functional connectivity modeling can improve EEG-based discrimination between tumor and healthy control subjects. Graph EEG Net-Lite achieved 96.2% accuracy, 96.8% sensitivity, 95.5% specificity, 95.9% F1-score, and an AUC of 0.987, while reducing the number of parameters by 74.8% compared with a standard GNN. These findings suggest that lightweight graph learning can provide a useful balance between predictive performance, computational efficiency, and interpretability.

The new framework does not replace MRI and CT; they are still needed for anatomical confirmation, tumor localization, tumor grading, and treatment planning. Therefore, the new framework is classified only as a non-invasive, auxiliary method for screening and decision support that may assist in high-risk cases, allowing prioritization of patients for later neuroimaging evaluation when repeated imaging is expensive, unavailable, and/or difficult to obtain.

The explainability analysis performed with the GNNExplainer showed strong contributions from the frontal, temporal, parietal, and occipital electrode regions to the model's output. However, these findings should be viewed only as electrode-level patterns of functional importance, not as direct localisations of the tumors. Future studies should include more extensive, multicentre datasets to validate the model, add tumor subtype and grade classification, compare static and dynamic connectivity graphs, and combine EEG findings with imaging-confirmed clinical metadata. Overall, this study suggests that using lightweight explainable EEG graph learning in this manner holds promise as a direction for advancing the accessibility of neurodiagnostic screening research.

Competing Interest Statement

The authors declare no known competing financial interests or personal relationships that could have influenced the work reported in this paper.

Data Availability Statement

The EEG recordings analyzed in this study originated from the clinical dataset described by Selvam and Shenbaga Devi [39] (DOI: 10.1515/msr-2015-0030) and were provided to the authors by a research collaborator. The present study used a 50-subject subset of the original clinical cohort, comprising 25 participants with radiologically confirmed brain tumors and 25 neurologically healthy controls; the complete original cohort was not used in the present analysis. The underlying EEG recordings are not hosted in an identified public repository, and the authors are not authorized to redistribute the raw data. Consequently, the raw recordings are not publicly available through this article. Requests for access should be directed to the data owners or the corresponding author of the original study and are subject to their permission and any applicable ethical and institutional restrictions.

Ethics Approval Statement

The EEG recordings analyzed in this study were collected previously as part of the clinical investigation reported by Selvam and Shenbaga Devi [39]. The source study states that data collection at the Institute of Neurology, Madras Medical College, Chennai, was conducted with approval from the institute's Ethics Committee. The present work constitutes a secondary computational analysis of previously acquired EEG recordings and involved no new participant recruitment, participant contact, or data acquisition. The authors of the present study do not have additional original consent documentation beyond the information reported in the source study.

References

[1] G. Yuan *et al.*, "Global, regional, and national burden of brain and other central nervous system cancers from 1990 to 2021, and projections to 2035: A systematic analysis for the Global Burden of Disease Study 2021," *International Journal of Surgery,* vol. 112, no. 1, pp. 286–302, 2026, doi: 10.1097/JS9.0000000000003497.

[2] M. C. M. Peeters, H. Zwinkels, J. A. F. Koekkoek, M. J. Vos, L. Dirven, and M. J. B. Taphoorn, "The impact of the timing of health-related quality of life assessments on the actual results in glioma patients: A randomized prospective study," *Cancers*, vol. 12, no. 8, Art. no. 2172, Aug. 2020, doi: 10.3390/cancers12082172.

[3] A. F. Eichler and S. R. Plotkin, "Brain metastases," *Current Treatment Options in Neurology*, vol. 10, no. 4, pp. 308–314, Jul. 2008, doi: 10.1007/s11940-008-0033-x.

[4] X. Liu *et al.*, "Current evidence and challenges of multitarget anti-angiogenic agents for glioblastoma: Results from clinical trials," *iScience*, vol. 28, no. 113521, pp. 1–24, 2025, doi: 10.1016/j.isci.2025.113521.

[5] J. Rafanan, N. Ghani, S. Kazemeini, A. Nadeem-Tariq, R. Shih, and T. A. Vida, "Modernizing neuro-oncology: The impact of imaging, liquid biopsies, and AI on diagnosis and treatment," *International Journal of Molecular Sciences,* vol. 26, no. 3, Jan. 2025, doi: 10.3390/ijms26030917.

[6] S. Kim *et al.*, "Global burden of brain and central nervous system cancer in 185 countries, and projections up to 2050: A population-based systematic analysis of GLOBOCAN 2022," *Journal of neuro-oncology,* vol. 175, no. 2, pp. 673–685, Nov. 2025, doi: 10.1007/s11060-025-05164-0.

[7] S. Singh *et al.*, "Glioblastoma at the crossroads: Current understanding and future therapeutic horizons," *Signal transduction and targeted therapy,* vol. 10, no. 1, Art. no. 213, Jul. 2025, doi: 10.1038/s41392-025-02299-4.

[8] M. Ijaz *et al.*, "Diagnostics of brain tumor in the early stage: Current status and future perspectives," *Biomaterials Science,* vol. 13, no. 10, pp. 2580–2605, 2025, doi: 10.1039/D4BM01503G.

[9] O. E. Yri *et al.*, "Survival and quality of life after first-time diagnosis of brain metastases: A multicenter, prospective, observational study," *The Lancet Regional Health–Europe,* vol. 49, no. 101181, 2025, doi: 10.1016/j.lanepe.2024.101181.

[10] V. Podder *et al.*, "Gaps in diagnosis, treatment, and outcomes among patients with brain tumors in the United States: A state-of-the-art review," *Cancers*, vol. 17, no. 3982, Dec. 2025, doi: 10.3390/cancers17243982.

[11] H. A. Mutar, S. M. M. Najeeb, M. L. Aldabag, and H. T. Salim, "Hybrid neural network-genetic algorithm framework for EEG and ECG signal classification," *Journal of Machine and Computing*, vol. 6, no. 1, pp. 280–295, 2026, doi: 10.53759/7669/jmc202606021.

[12] S. Abadal *et al.*, "Graph neural networks for electroencephalogram analysis: Alzheimer's disease and epilepsy use cases," *Neural Networks,* vol. 181, Art. no. 106792, Jan. 2025, doi: 10.1016/j.neunet.2024.106792.

[13] S. M. A. Rahman *et al.*, "Advancement in graph neural networks for EEG signal analysis and application: A review," *IEEE Access*, vol. 13, pp. 50167–50187, 2025, doi: 10.1109/ACCESS.2025.3549120.

[14] A. Belhadi, P. G. Lind, Y. Djenouri, and A. Yazidi, "Enhanced visibility graph for EEG classification," *Frontiers in neuroscience*, vol. 19, no. 1541062, May 2025, doi: 10.3389/fnins.2025.1541062.

[15] H. Mohammadi and W. Karwowski, "Graph neural networks in brain connectivity studies: Methods, challenges, and future directions," *Brain Sciences,* vol. 15, no. 1, Art. no. 17, 2025, doi: 10.3390/brainsci15010017.

[16] J. Li *et al.*, "Deep learning-powered electrical brain signals analysis: Advancing neurological diagnostics," *IEEE Reviews in Biomedical Engineering,* vol. 19, pp. 337–351, 2026, doi: 10.1109/RBME.2025.3625973.

[17] C. Cook, A. Auwal, S. Eglese, B. Hywel, M. A. Ellul, and B. D. Michael, "Real-world evaluation of an automated EEG spike detection software in a tertiary center compared to a clinical reference standard," *Journal of Neurology*, vol. 273, no. 2, p. 108, 2026, doi: 10.1007/s00415-026-13636-0.

[18] H. Uyanik, A. Sengur, M. Salvi, R.-S. Tan, J. H. Tan, and U. R. Acharya, "Automated detection of neurological and mental health disorders using EEG signals and artificial intelligence: A systematic review," *Wiley Interdisciplinary Reviews: Data Mining and Knowledge Discovery*, vol. 15, no. 1, Art. no. e70002, Mar. 2025, doi: 10.1002/widm.70002.

[19] R. Sharma and H. K. Meena, "Emerging trends in EEG signal processing: A systematic review," *SN Computer Science,* vol. 5, no. 4, Art. no. 415, Apr. 2024, doi: 10.1007/s42979-024-02773-w.

[20] P. Khan *et al.*, "Machine learning and deep learning approaches for brain disease diagnosis: Principles and recent advances," *IEEE Access*, vol. 9, pp. 37622–37655, 2021, doi: 10.1109/ACCESS.2021.3062484.

[21] M. Gavaret, A. Iftimovici, and E. Pruvost-Robieux, "EEG: Current relevance and promising quantitative analyses," *Revue Neurologique,* vol. 179, no. 4, pp. 352–360, Apr. 2023, doi: 10.1016/j.neurol.2022.12.008.

[22] S. J. J. Jui, R. C. Deo, P. D. Barua, A. Devi, J. Soar, and U. R. Acharya, "Application of entropy for automated detection of neurological disorders with electroencephalogram signals: A review of the last decade (2012–2022)," *IEEE Access*, vol. 11, pp. 71905–71924, 2023, doi: 10.1109/ACCESS.2023.3294473.

[23] A. Konkar and X. Qu, "A review of transformer-based and hybrid deep learning approaches for EEG analysis," in *HCI International 2025 – Late Breaking Papers*, H. Mori, Y. Asahi, D. D. Schmorrow, and C. M. Fidopiastis, Eds. Cham, Switzerland: Springer Nature Switzerland, 2026, pp. 391–404, doi: 10.1007/978-3-032-12660-3_29.

[24] C. Madhumitha and S. M. D. M, "Hybrid CNN-LSTM framework for accurate detection and classification of

epileptic seizures using EEG signals," in *Proc. 3rd International Conference on Intelligent Cyber Physical Systems and Internet of Things (ICoICI)*, Sep. 2025, pp. 473–477, doi: 10.1109/ICoICI65217.2025.11252809.

[25] S. T. Jonna and K. Natarajan, "EEG signal processing in neurological conditions using machine learning and deep learning methods: A comprehensive review," *The European Physical Journal Special Topics,* vol. 234, no. 15, pp. 3981–3999, Oct. 2025, doi: 10.1140/epjs/s11734–025-01606-y.

[26] D. Klepl, M. Wu, and F. He, "Graph neural network-based EEG classification: A survey," *IEEE Transactions on Neural Systems and Rehabilitation Engineering*, vol. 32, pp. 493–503, 2024, doi: 10.1109/TNSRE.2024.3355750.

[27] L. Cai *et al.*, "MM-GTUNets: Unified multi-modal graph deep learning for brain disorders prediction," *IEEE Transactions on Medical Imaging*, vol. 44, no. 9, pp. 3705–3716, 2025, doi: 10.1109/TMI.2025.3556420.

[28] H. A. Manan, E. A. Franz, and N. Yahya, "Functional connectivity changes in patients with brain tumors—A systematic review on resting state fMRI," *Neurology, Psychiatry and Brain Research,* vol. 36, pp. 73–82, Jun. 2020, doi: 10.1016/j.npbr.2020.03.003.

[29] E. S. Semmel, T. R. Quadri, and T. Z. King, "Graph theoretical analysis of brain network characteristics in brain tumor patients: A systematic review," *Neuropsychology review*, vol. 32, no. 3, pp. 651–675, Sep. 2022, doi: 10.1007/s11065-021-09512-5.

[30] V. Ronca *et al.*, "Beyond the lab: real-world benchmarking of wearable EEGs for passive brain-computer interfaces," *Brain Informatics*, vol. 13, no. 1, p. 3, 2026, doi: 10.1007/s40708-025-00276-9.

[31] F. A. Jibon *et al.*, "Sequential graph convolutional network and DeepRNN-based hybrid framework for epileptic seizure detection from EEG signal," *Digital Health,* vol. 10, Art. no. 20552076241249874, Sep. 2024, doi: 10.1177/20552076241249874.

[32] M. M. Rahman, V. Calhoun, and S. Plis, "Deep learning interpretability in neuroimaging: A comprehensive survey and methodological recommendations," *Imaging Neuroscience,* vol. 4, no. IMAG.a.1129., 2026, doi: 10.1162/IMAG.a.1129.

[33] M. Nandan, S. Mitra, and D. De, "GraphXAI: A survey of graph neural networks (GNNs) for explainable AI (XAI)," *Neural Computing and Applications,* vol. 37, no. 17, pp. 10949–11000, Jun. 2025, doi: 10.1007/s00521-025-11054-3.

[34] U. R. Acharya, S. V. Sree, G. Swapna, R. J. Martis, and J. S. Suri, "Automated EEG analysis of epilepsy: A review," *Knowledge-Based Systems,* vol. 45, pp. 147–165, Jun. 2013, doi: 10.1016/j.knosys.2013.02.014.

[35] V. J. Lawhern, A. J. Solon, N. R. Waytowich, S. M. Gordon, C. P. Hung, and B. J. Lance, "EEGNet: A compact convolutional neural network for EEG-based brain–computer interfaces," *Journal of neural engineering,* vol. 15, no. 5, Art. no. 056013, Jul. 2018, doi: 10.1088/1741-2552/aace8c.

[36] P. Bashivan, I. Rish, M. Yeasin, and N. Codella, "Learning representations from EEG with deep recurrent-convolutional neural networks," 2015, *arXiv preprint arXiv:1511.06448*, doi: 10.48550/arXiv.1511.06448.

[37] T. Song, S. Liu, W. Zheng, Y. Zong, and Z. Cui, "Instance-adaptive graph for EEG emotion recognition," *Proceedings of the AAAI Conference on Artificial Intelligence,* vol. 34, no. 03, pp. 2701–2708, Apr. 2020, doi: 10.1609/aaai.v34i03.5656.

[38] K. Kumar, "An effective epileptic seizure detection using graph neural networks," *Journal of Information Systems Engineering and Management,* vol. 10, no. 2s, pp. 157–166, Jan. 2025, doi: 10.52783/jisem.v10i2s.210.

[39] V. S. Selvam and S. S. Devi, "Analysis of Spectral Features of EEG signal in Brain Tumor Condition," *Measurement Science Review*, vol. 15, no. 4, pp. 219–225, 2015, doi: 10.1515/msr-2015-0030.

[40] I. Goodfellow, Y. Bengio, and A. Courville, Deep Learning. Cambridge, MA, USA: MIT Press, 2016.

[41] S. R. Saeed, A. H. Mohammed, S. K. Khaleel, and A. A. Al-Hilali, "The study of deep learning for automotive logo recognition and classification," *Periodicals of Engineering and Natural Sciences,* vol. 11, no. 3, pp. 255–268, 2023, doi: 10.21533/pen.v11.i3.151.

[42] M. A. Moh, Y. Y. Al-Aboosi, H. A. Abdualnabi, and H. Y. Al-Aboosi, "Optimized denoising of ECG and EEG signals using Discrete Wavelet Transform: A comparative study of wavelet types and thresholding techniques," *Interdisciplinary Journal of Health Environment and Computation*, vol. 1, no. 3, pp. 46–69, 2026, doi: 10.65983/ijhec.2026.03.0005.

[43] J. Chen *et al.*, "A review of EEG-based driver fatigue detection: Nonlinear dynamics, brain networks, and deep learning advances," *Wiley Interdisciplinary Reviews: Data Mining and Knowledge Discovery*, vol. 16, no. 2, Art. no. e70099, 2026, doi: 10.1002/widm.70099.

[44] M. S. Shareef, T. Abd, and Y. S. Mezaal, "Gender voice classification with huge accuracy rate," *TELKOMNIKA (Telecommunication Computing Electronics and Control),* vol. 18, no. 5, pp. 2612–2617, Oct. 2020, doi: 10.12928/TELKOMNIKA.v18i5.13717.